

Theo yêu cầu của khách hàng, trong một năm qua, chúng tôi đã dịch qua 16 môn học, 34 cuốn sách, 43 bài báo, 5 sổ tay (chưa tính các tài liệu từ năm 2010 trở về trước) Xem ở đây

**DỊCH VỤ
DỊCH
TIẾNG
ANH
CHUYÊN
NGÀNH
NHANH
NHẤT VÀ
CHÍNH
XÁC
NHẤT**

Chỉ sau một lần liên lạc, việc dịch được tiến hành

Giá cả: có thể giảm đến 10 nghìn/1 trang

Chất lượng: Tạo dựng niềm tin cho khách hàng bằng công nghệ 1. Bạn thấy được toàn bộ bản dịch; 2. Bạn đánh giá chất lượng. 3. Bạn quyết định thanh toán.

Tài liệu này được dịch sang tiếng việt bởi:

www.mientayvn.com

Từ bản gốc:

<https://drive.google.com/file/d/0B4rAPqlxIMRDY2tRd2UxO3lweiO/view?usp=sharing>

Liên hệ dịch tài liệu :

thanhlam1910_2006@yahoo.com hoặc frbwrthes@gmail.com hoặc số 0168 8557 403 (gặp Lâm)

Tìm hiểu về dịch vụ: http://www.mientayvn.com/dich_tieng_anh_chuyen_nghanh.html

5.2 Three Case Studies 1 h

This chapter focuses on studying the behavior of a non-solitonic pulse (a Gaussian pulse) propagates in a stable nonlinear periodic structure. The steady-state analysis of this device [11] revealed

5.2 Ba trường hợp cần xét (ba nghiên cứu tình huống)

Chương này tập trung nghiên cứu đặc tính của xung phi soliton (xung Gauss) truyền trong một cấu trúc tuần hoàn phi tuyến ổn định. Qua phép phân tích trạng thái xác lập (ổn định), chúng ta thấy các

its stable limiting characteristic where the transmitted intensity I_{tran} is independent of high incident intensity I_{in} for cw inputs, and the function $I_{\text{tran}}(I_{\text{in}})$ is an one-to-one function (i.e., one input corresponds to only one output). In the case of a perfectly balanced nonlinearity, $n_{\text{nl}} = 0$, it is proven in [11] that the grating operates in the stable limiting regime for both the in-phase ($n_{0k} > 0$) and out-of-phase ($n_{0k} < 0$) cases.

In this chapter, three cases in the stable regime are studied with pulse inputs to explore the instantaneous temporal response of the device:

(i) no linear built-in grating ($n_{0k} = 0$) with balanced Kerr coefficients ($n_{\text{nl}} = 0$),

Built-in: tích hợp sẵn, có sẵn, đã tồn tại

(ii) in-phase built-in grating ($n_{0k} > 0$) with balanced Kerr coefficients ($n_{\text{nl}} = 0$),

(iii) out-of-phase grating ($n_{0k} < 0$) with balanced Kerr coefficients ($n_{\text{nl}} = 0$).

In all three examples, the consideration of balanced Kerr coefficients implies that the average index of the grating remains fixed even as the pulse propagates through. The position of the center of the stopband (dải chặn, dải chắn) therefore remains fixed, and it is the amplitude of the grating, and its relationship with the built-in linear grating amplitude, which varies.

5.3 Case (i): No Linear Grating with Balanced Non-linearity ($n_{0k} = 0$ and $n_{\text{nl}} = 0$)

Figure 5.1 illustrates the refractive index profile of the Bragg grating structure with alternating layers of materials with identical linear refractive indices and

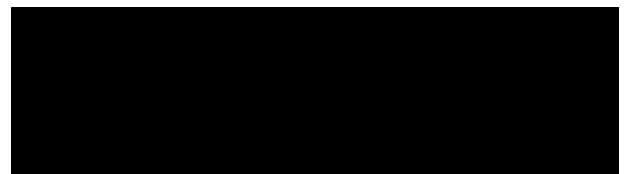
tính chất giới hạn cường độ ổn định của thiết bị trong đó cường độ truyền qua... không phụ thuộc vào cường độ tới... đối với các đầu vào liên tục, và hàm... là hàm một-một (tức là một đầu vào tương ứng với một đầu ra). Trong trường hợp cân bằng phi tuyến hoàn hảo,..., người ta chứng minh rằng [11] cách tử hoạt động trong chế độ giới hạn cường độ ổn định đối với cả trường hợp đồng pha và lệch pha

Trong chương này, chúng ta sẽ nghiên cứu ba trường hợp trong chế độ ổn định với các đầu vào xung để khảo sát đáp ứng thời gian tức thời của thiết bị:

(i) không có cách tử tuyến tính built-in với các hệ số Kerr cân bằng....

(ii) Cách tử built-in đồng pha.... với các hệ số Kerr cân bằng

(iii) Cách tử lệch pha.... với các hệ số Kerr cân bằng



oppositely- signed Kerr coefficients, i.e., $n_{0k} = 0$ and $n_{1l} = 0$. The steady-state analysis of this device is described in Figure 5.2, and shows the transmittance as a function of incident intensity. The inset of Figure 5.2 illustrates limiting behavior, wherein the intensity of the transmitted light is clamped, approaching asymptotically the limiting intensity as incident intensity increases. What happens when a ultrashort pulse is incident onto the device instead of a cw wave? Will the device demonstrate limiting behavior? Will the device display other interesting functionalities? The following sections will address these questions.

Figure 5.1: Profile of the linear refractive indices and Kerr coefficients of the device along the device length for case study (i). The refractive indices of the two adjacent layers are

5.3.1 Optical Limiting

For comparison, similar device parameters as in the steady-state analysis (nonlinearity, length, and periodicity) are applied to investigate the instantaneous temporal response of the structure. Instead of the cw inputs as in the steady-state analysis, pulses which take the form of (4.12) are introduced for the following time-domain study. These pulses have a fixed transform-limited width (độ rộng xung cực tiểu khả dĩ của một phổ quang học nào đó) of 605 fs with different peak intensities (cường độ peak, cường độ đỉnh) to give varying energies. This pulse width corresponds to a spectral bandwidth of 1.6 THz which is smaller than the maximum bandwidth of the stopband created by the nonlinear grating, i.e., $\Delta\omega \sim \omega = 1.7$ THz.

Figure 5.3 illustrates the energy

transmittance as a function of incident pulse energy. The term 'energy transmittance' is defined in a similar way to the intensity transmittance in the cw case: it is the ratio of the total transmitted energy density W_{tran} to the total incident pulse energy density W_{in} , where the energy densities are defined in Eq. (4.11). The peak intensities of the transmitted pulses are also recorded, and plotted in the inset of Figure 5.3. The limiting behavior demonstrated in this figure closely resembles the steady-state response reported in Figure 5.2. The limiting effect

Figure 5.2: Steady state analysis:

Transmittance as a function of incident intensity for various device lengths: $L = 70 \text{ } \mu\text{m}$, $180 \text{ } \mu\text{m}$ and $290 \text{ } \mu\text{m}$. Inset: transmitted intensity level versus incident intensity for the same device, demonstrating characteristic limiting behavior.

is less pronounced for energy. However, in contradistinction with steady-state average power results, the time-domain transmitted energy is not asymptotically limited. For very low incident peak intensities the refractive indices of the two adjacent layers are matched. Thus the device is transparent to the incoming light, resulting in a close-to-unity transmittance. Increasing the intensity causes the indices to change, which creates a grating, leading to reflection. As the peak intensity (cường độ peak, cường độ cực đại, cường độ tại đỉnh xung) of the incident pulse increases further, the peak intensity of the transmitted pulse eventually approaches a limiting intensity. Figure 5.3 also illustrates the decreasing limiting intensity with



increasing number of periods (longer devices). The transmitted peak intensity of a 605 fs pulse is shown to be limited roughly at 1.2, 1.6, and 2.8 GW/cm² for a 290, 180, and 70 μ m-long device, respectively.

The results presented in Figure 5.3 are for fixed incident pulse width. In contrast, Figure 5.4 illustrates the energy transmittance as a function of pulse width, given that the incident peak intensity remains constant. In these numerical computations, the incident pulse again takes the form of (4.12) with a fixed peak pulse intensity of $I_{\text{peak}} = 4$ GW/cm², such that the maximum magnitude of change in the refractive index is equal to the chosen 0.01. The graph displays the limiting behavior of the pulse transmission and the bandwidth dependence of the transmission.

Long-duration pulses in Figure 5.4 exhibit the desired limiting behavior because their spectral bandwidth lies entirely inside the stopband of the grating, leading to bandwidth-independent transmittance. Short-duration pulses, on the other hand, have a spectral bandwidth which exceeds the width of the dynamic stopband, resulting in transmission of the portion of the power which lies outside of the stopband of the device. In the limit of short pulse duration, the pulse bandwidth is wide enough that most of its power lies outside the nonlinear stopband; hence the pulse transmittance approaches unity. The knee in the characteristic of Figure 5.4 occurs when the pulse bandwidth and nonlinear stopband bandwidth become comparable: In Figure 5.4, the transmittance decreases from 0.75 to 0.25 when the device length is increased from 70 μ m to 290 μ m. The

pulse intensity decays as the pulse evanesces along the length of the device.

We now consider the case of pulses of fixed energy, where the intensity and temporal width are co-varied to satisfy this constraint. The spectral bandwidth ($1/\text{FWHM}$) increases with the same proportionality as the bandwidth of the grating ($\propto \sqrt{L/\lambda}$). If a given pulse has a peak intensity, bandwidth, and L/λ combination such that the pulse bandwidth lies within the nonlinear grating bandwidth, then it will continue to do so when a second pulse of the same energy with narrower temporal width and higher in peak intensity.

In summary, an optical limiter may be designed which will guarantee that its output peak intensity will be less than a required intensity. This is achieved through the choice of the number of layers, peak intensity, and temporal width. It is observed that the time-domain transmitted energy is not asymptotically limited as in the steady-state case. It is also noted that the limiter does not require large number of layers. For instance, the transmitted peak intensities of a 605 fs incident pulse (with a characteristic length of 180 μm) are less than 1.2, 1.6, 2.8 GW/cm^2 for a device length of 290 μm , 180 μm and 70 μm , respectively.

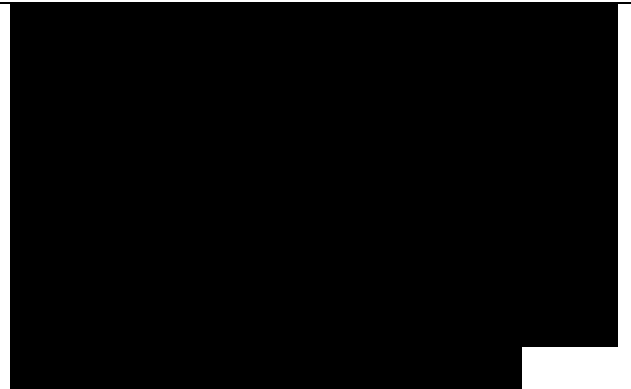
5.3.2 Pulse Shaping

In Section 4.5, Figure 4.2 illustrated the non-solitonic character of Gaussian pulse propagation through a balanced nonlinear structure with constant linear indices ($n_0k = 0$ and $n_{nl} = 0$). Both the amplitude and the shape of the Gaussian

pulse were distorted. The shape of the transmitted pulse depended on the size of the structure and the initial pulse width. Figure 5.5 shows the transmitted pulse shapes through a 180 μm -long device for two different temporal widths. The input Gaussian pulses are 605 fs wide in Figure 5.5(a) and 1440 fs wide in Figure 5.5(b), and both have a 4 GW/cm² peak intensity.

The bandwidth of both pulses is much less than the effective bandwidth of the device, allowing us to focus attention on intensity self-patterning of the pulses and to remove the effects of incomplete spectral blocking. To explain the distortion in the transmitted pulses, the time-dependent transmittance of the induced nonlinear grating is calculated, and illustrated in Figure 5.6(a) and 5.6(b). For the shorter pulse length of 180 μm , Figure 5.6(a) shows that the forward- and backward-propagating waves form their strongest instantaneous gratings at different times. The backward-propagating wave gives rise to an additional delayed replica of the transmitted pulse in the time-dependent transmittance, causing the dip in the transmitted pulse of Figure 5.5(a). When the incident pulse is longer than the device (435 μm in this example), the strongest instantaneous gratings are formed roughly at the same time for forward- and backward-propagating waves (Figure 5.6(b)). Sequential multiple reflections of pulses inside the relatively short structure create echoed patterning of the transmitted pulse seen in Figure 5.5(b).

Figure 5.5: Input and output intensities of a pulse propagating through a 180 μm -



long device for an input pulse width of: (a) 605 fs or characteristic length of 180 μm and (b) 1440 fs or characteristic length of 435 μm .

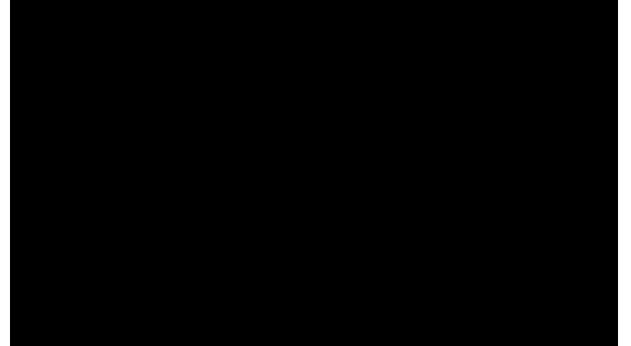
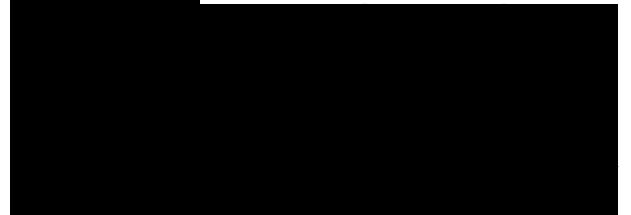
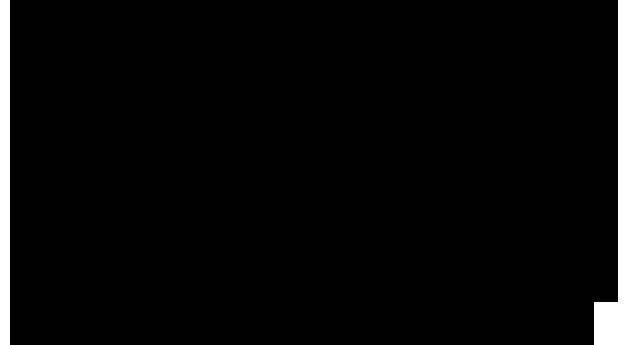
Figure 5.6: Heuristic analysis of pulse shaping in a 180 μm -long nonlinear grating. The time dependent instantaneous transmittance attributable to contributions from forward- and backward-propagating pulses for an input pulse width of: (a) 605 fs or characteristic length of 180 μm and (b) 1440 fs or characteristic length of 435 μm .

5.4 Case (ii): In-phase Built-in Linear Grating with Balanced Nonlinearity ($n_{0k} > 0$ and $n_{1l} = 0$)

Linear refractive index n_0

Figure 5.7: Profile of the linear refractive indices and Kerr coefficients of the device along the device length for case study (ii). The refractive indices of the two adjacent layers are $n_{0i} + n_{1i}$ and $n_{02} + n_{12}$, where $n_{1i} = -n_{12}$.

We now consider periodic structures with an in-phase linear built-in grating such that $n_{0k} > 0$ and $n_{2k} > 0$, as illustrated in Figure 5.7. The intensity-induced nonlinear grating adds constructively to the existing built-in linear grating, resulting in low transmittance. No significant transmitted pulse energy is observed for a large range of different input pulses, since most of the incident light is blocked by the linear built-in grating. This is evident in the bottom curve of Figure 5.9(a), constructed for the in-phase linear grating with $n_{0k} = 0.01$, i.e. $n_{1,2} = (1.50 \pm 0.01) \pm (2.5 \times 10^{-12} \text{ GW/cm}^2)/\text{in}$.



5.5 Case (iii): Out-of-phase Built-in Linear Grating with Balanced Nonlinearity ($n_{0k} < 0$ and $n_{nl} = 0$)

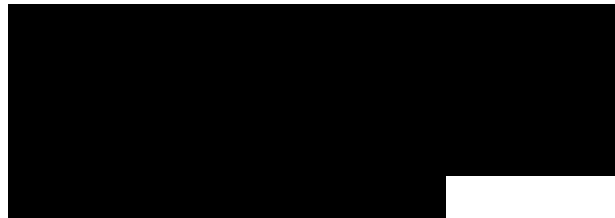
Linear refractive index n_0

Figure 5.8: Profile of the linear refractive indices and Kerr coefficients of the device along the device length for case study (iii). The refractive indices of the two adjacent layers are $n_{01} + n_{0,n}$ and $n_{02} + n_{0,I}$, where $n_{0,n} = -n_{0,I}$.

Here periodic structures with an out-of-phase linear built-in grating are considered, such that $n_{0k} < 0$ and $n_{2k} > 0$, as shown in Figure 5.8. The out-of-phase linear built-in grating allows for a dynamic balance with the intensity-induced nonlinear grating as the pulse propagates through the structure. When the intensity of the pulse exceeds that required to take the instantaneous nonlinear grating through the zero point and over to the other sign, the grating is bleached and then re-established as the incident pulse propagates through the structure.

5.5.1 S-curve and N-curve Transfer Characteristics

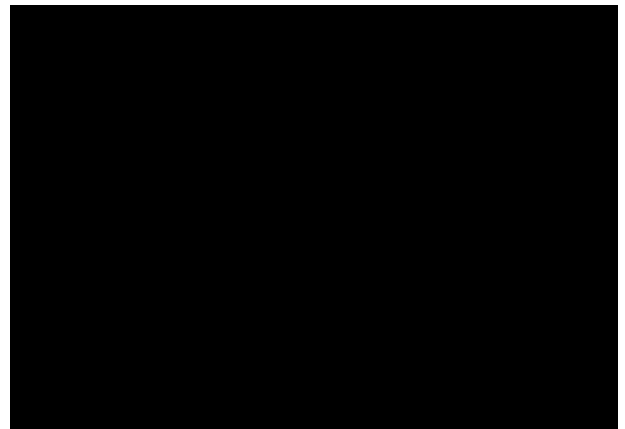
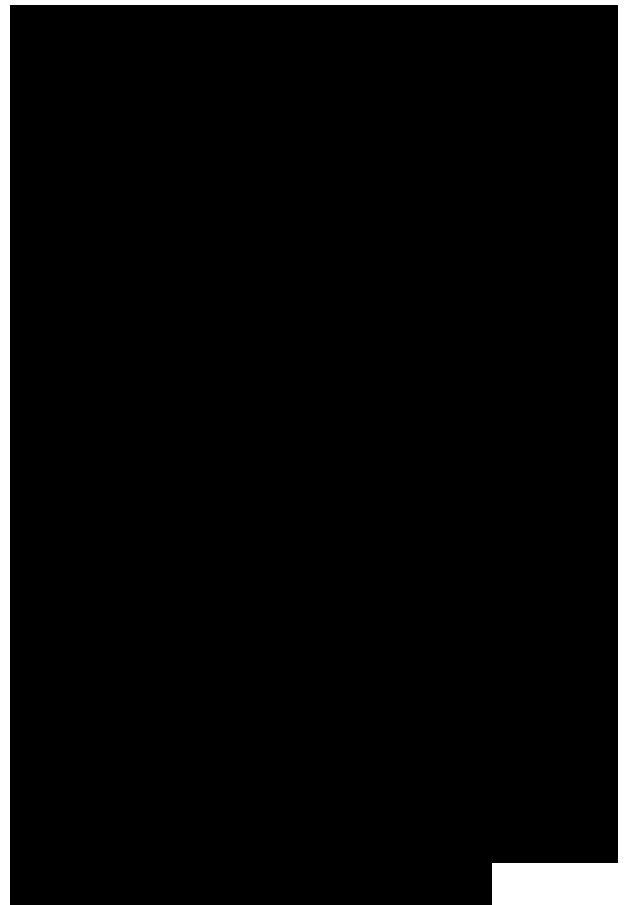
We begin by investigating the effects of grating strength on the transmittance of the device. In this analysis, a fixed incident pulse with width of 605 fs is launched at structures with linear out-of-phase gratings of $n_{0k} = -0.002$, $n_{0k} = -0.005$, and $n_{0k} = -0.01$. The intensity $I_c = |n_{0k}|/n_{2k}$ which causes the nonlinear index change to balance completely with the out-of-phase linear grating, is referred to as the closing intensity. When the balance between linear and nonlinear grating closes the overall grating profile, the device is



locally transparent. The total transmitted pulse energy density versus the total incident pulse energy density is shown in Figure 5.9(a) for the out-of-phase linear gratings listed above. The pulse energy transmittance is shown in Figure 5.9(b) for the same out-of-phase linear gratings.

When the out-of-phase linear grating is large enough to effect a significant built-in reflectance (for example, when the built-in linear index difference is 0.01), the transmittance reveals an interplay between built-in and intensity-dependent grating behavior. At small incident pulse intensities the linear built-in grating blocks most of the light, resulting in a close-to-zero transmittance. The transmittance gradually increases as the increasing intensity-induced nonlinear index change offsets the linear grating. The closing and reopening of the grating are responsible for the S-curve character of the transfer function in Figure 5.9(a), which may be used for optical logic gates such as an AND gate [31, 38]. The energy transmittance is at its maximum when the peak intensity of the incident pulse is at the closing intensity. Here the regions around the peak of the pulse bleach out the grating.

Long-duration pulses exhibit the limiting trend of Figure 5.9(b). However, the energy transmittance of linear built-in gratings does not converge to the case of constant linear index across the device: the more intense are the input pulses, the more there exist regions where the self-induced nonlinear grating matches with the built-in linear grating, and the transmittance is higher than that with no



linear grating.

Since the energy transmittance displays an interesting S-curve character for a grating strength of 0.01, this grating strength becomes the focus of the study. The transfer characteristics of the peak intensities are plotted in Figure 5.10. Unlike the one-step limiting characteristics as shown in the inset of Figure 5.3, the peak intensities of the

Energy density of input pulse (GJ/cm)

Figure 5.9: (a) Total pulse transmitted energy density versus total incident pulse energy density for linear in- and out-of-phase built-in gratings;

(b) Corresponding energy transmittance as a function of incident pulse energy. A pulse width of 605 fs and a device length of 180 μm were fixed for all cases.

Incident Pulse Peak Intensity (GW/cm²)

Figure 5.10: Transfer characteristics of pulse peak intensities for varying device lengths: (a) S-curve for the peak intensities of the transmitted pulses; (b) N-curve for the peak intensities of the reflected pulses. I_1 and I_2 are two threshold intensities. Incident pulses with a fixed width of 605 fs propagate through device length of 70 μm , 180 μm , and 290 μm . The device has a 0.01 out-of-phase linear grating.

transmitted and reflected pulses exhibit an S- (Figure 5.10(a)) and an N-curve character (Figure 5.10(b)), respectively. These characteristics are more obvious for longer devices.

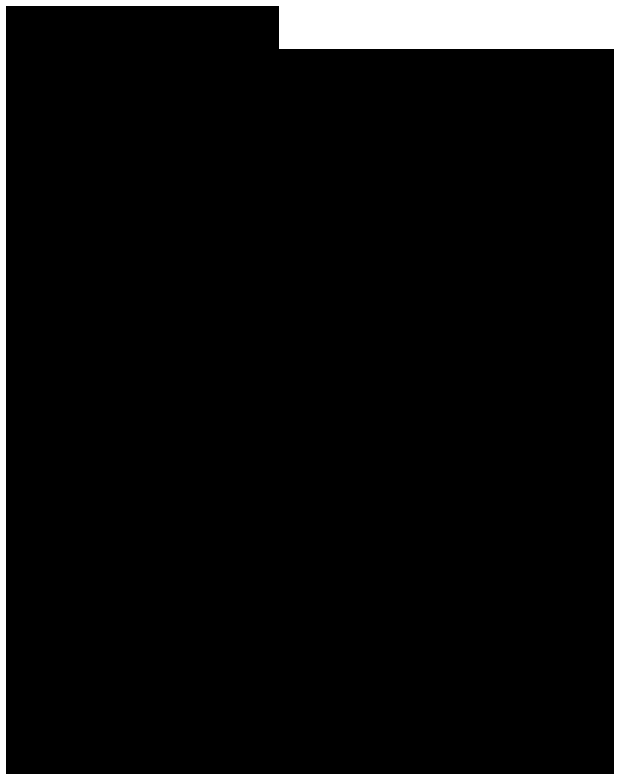
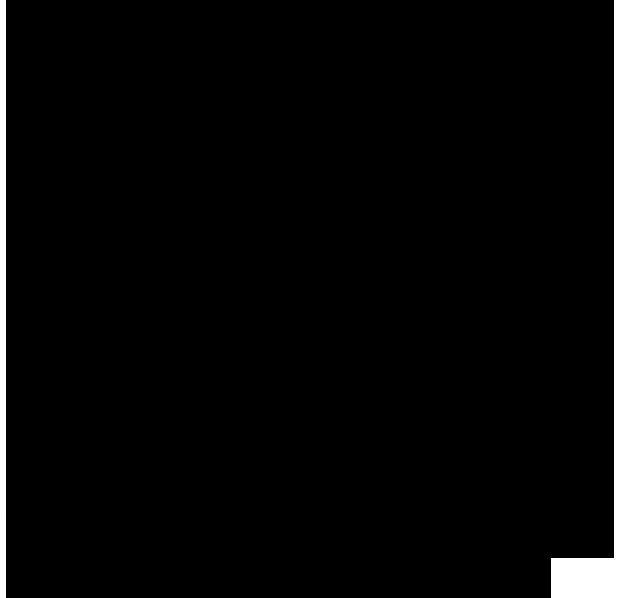


The S- and N-curve transfer characteristics can enable a complete logic set [31]. We consider the curve with the device length $L = 290 \text{ }^{\wedge}\text{m}$, for example: an incident pulse which is combined by 2 input pulses from a 3 dB coupler propagates through the nonlinear periodic structure with the S-curve transfer character. If a logic 1 is assigned to the peak intensity corresponding to $I > I_2$ in Figure 5.10(a) and a logic 0 is assigned to the peak intensities corresponding to $I < I_1$, an output will only be observed when both input pulses are present, i.e. $I_{in1}, I_{in2} > I_2$. This is an AND operation.

In summary, optical logic gates may be formed using a nonlinear periodic structure with a linear built-in grating. The longer the device, the better the functionalities. S- and N-curve transfer characteristics required for optical logic gates are observed.

5.5.2 Pulse Compression

We now proceed to examine the influence of device length on transmitted pulse shapes in the presence of an out-of-phase linear grating with $n_0k = -0.01$. The peak intensity of the incident pulse is fixed to $I_{peafc} = 4 \text{ GW/cm}^2$ to close the grating, and the pulse width is fixed at $\text{FWHM} = 605 \text{ fs}$. The initial stage of the pulse compression, reshaping and high-amplitude multiple-peak oscillation effects are shown in Figure 5.11 for different device lengths. A maximum of 88% pulse compression is observed for a $720 \text{ }^{\wedge}\text{m}$ -long device. This process resembles Gaussian pulse propagation in the out-of-phase linear gratings displayed in Figure 4.3. Figure 4.3 and Figure 5.11



differ only in the parameters used for the incident pulse. For a smaller peak intensity I_{peak} and larger pulse width, the pulse reshaping and multiple-peak oscillations in Figure 5.11 occur further into the device as compared to those in Figure 4.3. For this reason we study in detail the initial stage of pulse compression for $L < 300 \text{ } \mu\text{m}$, when the compressed Gaussian pulse preserves a single-peak shape.

It can be proven analytically that pulse compression can result from an out-of-phase built-in linear grating, assuming the incident pulse takes the form of (Eq. 4.12). For $t = 0$, zero initial conditions, and a real boundary value of $A_+(0, T) = \sqrt{J}/\ln(T)$, the coupled-mode system (3.19)-(3.20) can be simplified to

$$A_+ = u(Z, T), \quad A_- = iy(Z, T),$$

where u and y are real variables satisfying the system:

It follows from Eq. (5.3) if $n_0 k < 0$ that the time-derivative dy/dT is negative for $y \ll 0$ and $0 < u(T) < \sqrt{JTC_i}$. Here $|c_l| = |n_0 k|/n_2 k$ is the closing intensity. Therefore, when the Gaussian pulse (Eq. 4.12) enters the device at the input $Z = 0$, the generated backward wave (sóng ngược, sóng lùi, sóng phản hồi) field y is always negative. The other equation (5.2) defines the rate of change of the pulse amplitude in the reference frame moving to the right with unit speed (the speed of the Gaussian pulse). At the peak of the Gaussian pulse, the rate of change is positive if $y < 0$ and $I_{\text{peak}} > |c_l|$. Therefore, the Gaussian pulse with peak intensity I_{peak} exceeding the closing intensity $|c_l|$ is compressed in width and

increased in peak amplitude by the out-of-phase built-in linear grating. On the other hand, similar analysis shows that the Gaussian pulse with $I_{\text{peak}} < I_c$, or the Gaussian pulse in the in-phase built-in linear gratings with $n_0 k > 0$, is decompressed in width and decreased in amplitude during propagation in the nonlinear periodic structure.

To validate and explain the observation of pulse compression, we seek to reveal the evolution of the pulse, and consequently the instantaneous grating, in time and space across the device. Figure 5.12(a) shows the rate of change in amplitude of the forward propagating wave, or $\frac{dA^+}{dz}$, in a 180 μm -long device. As follows from Eq. (5.2), the forward-propagating wave is enhanced when the backward-propagating wave is coupled in. Moreover, the rate of change in amplitude of $A^+(z, T)$, or $\frac{dA^+}{dz}$, resembles the profile of the backward propagating envelope $A^-(z, T)$. The M-shaped graph along the time axis describes the existence of pulse propagation along the device length.

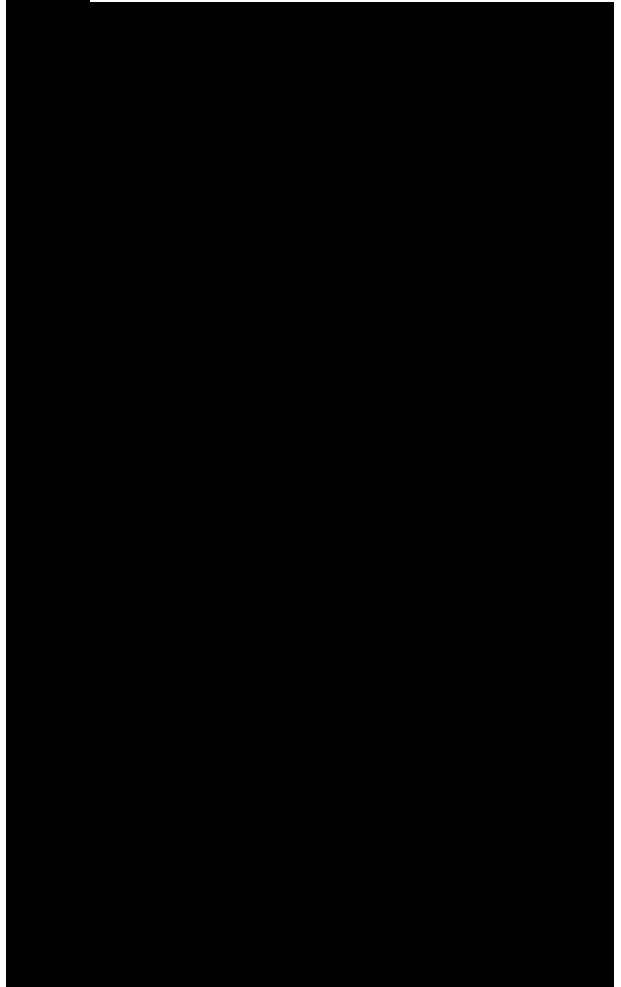
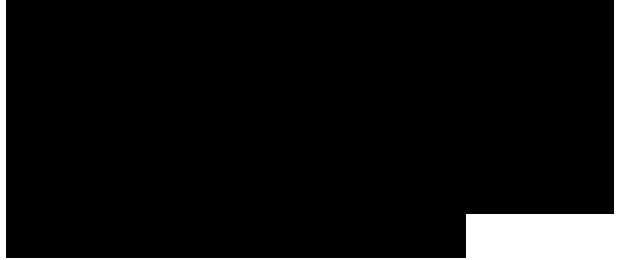
Figure 5.12(b) provides insight into the mechanism of pulse compression. In Figure 5.12(c) we compare a reference input pulse to a compressed pulse. The slopes of the amplitude of the compressed envelope is smaller than that of the reference Gaussian pulse at the beginning stages of a compressing process (up to time $t = a$). The slopes of the compressed pulse then increases dramatically before reaching the peak. The slopes of the compressed pulse is bigger than that of the reference pulse at the range time $c < t < b$.

Figure 5.12: (a) Rate of change in amplitude of the forward propagating

wave; (b) top view of (a); (c) a simplified intensity diagram of an incident pulse and a compressed pulse; (d) a plot of the intensity of the propagating wave in time and space. A pulse with $I_{\text{peak}} = 4 \text{ GW/cm}^2$ and $\text{FWHM} = 605 \text{ fs}$ is launched into the input of a $180 \text{ } \mu\text{m}$ -long device.

Similar arguments apply to the second half of the compressed pulse, except the slopes of the compressed envelope are smaller compared to the reference pulse at time $b < t < c$, and bigger after $t = c$ at the final stages of the compressing process. The convergence of the four slopes of the M-shape along the device length in Figure 5.12(b) shown by the four orange solid lines implies pulse compression.

As the pulse propagates through the structure, the intensity-induced nonlinear grating gradually offsets the existing linear built-in grating, reaching a 0 total grating. The sum of forward- and backward-propagating intensities can give rise to an instantaneous peak intensity which exceeds that required to close the grating completely at some time instances. For a short period of time the nonlinear grating dominates the index grating, which creates a slight in-phase total grating (positive values). Figure 5.12(d) depicts this process in a 500-layer ($180 \text{ } \mu\text{m}$ long) device. The front of the pulse travels approximately at the same speed as the peak of the pulse. The trailing edge, however, catches up with the leading edge, resulting in pulse compression. The effect resembles the pushbroom effect described in both [6] and [7]. Here, however, instead of using both pump signal and probe beam, only



one strong pulse is used to alter the local refractive index of the medium - resulting in a self-induced pushbroom effect.

The compression effects are observed when the peak pulse intensity I_{peak} is set to close completely the grating, i.e. $I_{peak} = I_{c1} = |n^o_k|/n_2k$. If the intensity-induced nonlinear grating is small compared to the out-of-phase linear grating, the transmittance is expected to be lower due to reflection by the grating. A pulse (give by Eq. 4.12) with peak intensity $I_{peak} = 2 \text{ GW/cm}^2$ chosen to give a maximum nonlinear grating of 0.005 (lower than the out-of-phase linear built-in grating $n^o_k = -0.01$) is simulated. In the case of a higher input peak intensity I_{peak} , the nonlinear grating will dominate the grating profile, resulting in a switching of the sign of the grating profile. Similar to the $I_{peak} = 4 \text{ GW/cm}^2$ case, the energy of forward- and backward- propagating waves will be stored inside the grating, causing pulse compression during transmission. Figure 5.13(b) shows the compressed output pulse simulated when the peak incident pulse is $I_{peak} = 6 \text{ GW/cm}^2$ which provides a maximum induced nonlinear grating of 0.015 (higher than the out-of-

Figure 5.13: Transmitted pulse (output) shapes when the intensity of the incident Gaussian pulse is set to: (a) $I_{peak} = 2 \text{ GW/cm}^2$ and (b) $I_{peak} = 6 \text{ GW/cm}^2$. The width of the pulse is $\text{FWHM} = 605 \text{ fs}$ and the device length is fixed to $L = 180 \mu\text{m}$.

Summarizing, envelope compression in nonlinear optical structures with an out-of-phase built-in linear grating is observed when the device length does not exceed twice the input pulse width and the peak input intensity meets or exceeds that required to close the grating.

5.6 Summary

This chapter presented the results obtained from the simulations and performed a numerical analysis to investigate pulse propagation behavior in a nonlinear Bragg structure. Three cases of grating strength (i.e., no built-in grating, in-phase built-in grating, and out-of-phase grating) were examined. In the absence of the linear grating, the energy transmittance of pulses with small bandwidth (compared to the bandwidth of the grating) was independent of pulse width. The limiting behavior of the device was pulse-bandwidth-dependent. The mechanisms behind output pulse shape formation for long-duration pulses were distinguished from that for short-duration pulses. In the presence of the out-of-phase linear grating, S-curve transfer characteristics were observed due to the erasure and reopening of the stopband. A compression effect reminiscent of the pump-probe pushbroom effect for a single pulse was predicted and a mathematical proof for pulse compression was also provided.

The temporal analysis of the pulse propagation presented in this chapter explored the limiting, logic operations, and pulse reshaping functions of the nonlinear Bragg structure. An optical limiter was demonstrated to limit the transmitted peak intensity of a 605 fs pulse to 1.2, 1.6, and 2.8 GW/cm² for a 290, 180, and 70 μ m-long device, respectively. A 0.01 out-of-phase linear grating with a length of at least 180 μ m was observed to have an S- and an N-curve transfer characteristic. A 720 μ m-long device with the same out-of-phase

grating was shown to exhibit significant pulse compression, compressing a pulse to 12% of its original pulse width.

6.2 Significance of Work

This work represents the first time-domain analysis of the temporal response of a stable periodic structure with alternating layers of nonlinear materials with oppositely-signed Kerr coefficients. Prior to this work there existed no systematic study of nonlinear solitonic and non-solitonic pulse behavior in such stable Bragg structures. As a result of this work, the questions outlined earlier in Chapter 2 have been fully addressed and the answers are summarized here:

- **QUESTION:** In what ways do the proposed nonlinear Bragg structure provide an improvement to optical signal processing over previously considered devices?

ANSWER: The proposed nonlinear Bragg structure is complementary to the bistable optical switching devices such as nonlinear Fabry-Perot resonators. The structure was theoretically predicted to have the capability of achieving multiple optical signal processing functions including limiting (Sections 5.3 and 5.5), reshaping (Section 5.3), logic operations (Section 5.5), and pulse compression (Section 5.5).

- **QUESTION:** What are the important design issues in using nonlinear Bragg structures for practical optical signal processing?

ANSWER: The device parameters and pulse properties were chosen according to the experimental literature for nonlinear materials properties (Section 4.4.1). The

Kerr coefficients $n_{1,2}$ of the two adjacent layers were chosen to be $n_{1,2} = \pm 2.5 \times 10^{-12} \text{ cm}^2/\text{W}$, and the average linear index $(n_{01} + n_{02})/2$ was fixed at 1.50. The signal processing functions listed below used this range of parameters, as well as specifications for device length and incident pulse width.

— Optical limiting may be achieved through the choice of the number of layers, peak intensity, and temporal width. For example, a pulse with FWHM = 605 fs was found to limit its transmitted peak intensity to 1.2, 1.6, and 2.8 GW/cm² for a 800-, 500-, and 180-layered device (i.e., 290, 180, and 70 μm), respectively.

— An optical logic gate may be formed using a nonlinear periodic structure with a linear built-in grating. For example, a 0.01 out-of-phase linear grating (i.e., $n_{1,2} = (1.50 \pm 0.01) \pm 2.5 \times 10^{-12} \text{ in}$) with a device length of at least 180 μm was shown to have S- and N-curve transfer characteristics. It had previously proven that such transfer characteristics allow a complete set of logic operations.

— A pulse compressor may be designed by proper choice of the number of device layers and peak intensity. For example, a 720 μm -long device exhibited significant pulse compression, compressing a pulse down to 12% of its original width.

• QUESTION: How does the time-dependent (pulse-processing) behavior relate to the known steady-state responses?

ANSWER: The limiting behavior and the S-curve transfer character are present in both the time-dependent and the steady-state response. The erasure and reopening of the stopband were shown to be responsible for these characteristics. However, in contradistinction with the steady-state average power results, the time-domain transmitted energy is not asymptotically limited. Temporal pulse compression makes the device attractive for signal processing. Section 5.5.2 investigated this special effect.

• QUESTION: What differentiates solitonic from non-solitonic propagation?

ANSWER: A Bragg soliton propagates through a periodic structure in two coupled counter-propagating waves that maintain their shape; while a non-solitonic pulse propagates as a forward wave, then generates a reflected backward wave, and hence displays variations in pulse shape. In general, the strict requirements on peak power, initial pulse shape, and pulse duration needed to balance precisely the effects of dispersion and nonlinearity for producing a soliton may be difficult to satisfy. According to Chapters 3 and 4, the Bragg soliton that was induced in the structure (with $n_{i,2} = (1.50 \pm 0.01) \pm 2.5 \times 10_{-12}/\text{in}$) was required to have a peak intensity of 55 GW/cm² and a narrow pulse width of ~27 fs. The Gaussian pulse used for the equivalent structure took a much lower peak intensity of 4 GW/cm² and a much wider pulse width of ~605 fs.

Non-iterative Algorithm for Solving the CME System

The real functions $u, v, w,$ and y satisfy the coupled system in Eq. (4.2) are:

.....

We use Crank-Nicholson finite difference method to solve the above partial differential equations. In Eq. (4.6), the derivatives of the functions $u, v, w,$ and y are approximated. For example,

.....

The element u_a represents the value of the function u at the grid point ($Z = a\Delta z, T = P\Delta t$). This numerical method is known to be unconditionally stable for any values of $\Delta t, \Delta z,$ and $n^{\circ}k$ [11].

The nonlinear function $f_a(w,w,v,y)$ is defined by

The system (A.4) can be used to evaluate functions of $U_g, w^{\wedge}, v^{\wedge},$ and when $a = 1, 2, \dots, N$ and $3 = 1, 2, \dots, K$. The boundary values $u^{\circ}, v^{\circ}, y^{\circ}, u_{N+1}, v_{N+1}, y_{N+1}$ are considered separately. The boundary conditions in Eq. (4.8) state

The three-point forward difference method is used for solving $u, w, v,$ and y at the boundary $Z = 0$ and $z = L$.

We thus obtain a non-iterative algorithm for solving the functions at a specific time instance:

where

And the matrices $H_a(u, w, v,y), H_g(w,u,y, v), H^{\wedge}(v,y,u, w),$ and $H_g(y, v, w,u)$ are expressed as follows:

The linear system described in Eq. (A.14) is implemented to calculate the values of u, v, w, y at the time instance Δt .

--	--